Research articles

Development and application of measurement techniques for evaluating localised magnetic properties in electrical steel

N.J. Lewis [a,*], P.I. Anderson [a], Y. Gao [b], F. Robinson [c]

[a] Wolfson Centre for Magnetics, Cardiff University, School of Engineering, Cardiff CF24 3AA, UK
[b] Research and Development, Tata Steel, Coventry CV4 7HP, UK
[c] Cogent Power Ltd, Newport NP19 0RB, UK

ARTICLE INFO

ABSTRACT

This paper reports the development of a measurement probe which couples local flux density measurements obtained using the needle probe method with the local magnetising field attained via a Hall effect sensor. This determines the variation in magnetic properties including power loss and permeability at increasing distances from the punched edge of 2.4% and 3.2% Si non-oriented electrical steel sample. Improvements in the characterisation of the magnetic properties of electrical steels would aid in optimising the efficiency in the design of electric machines.
© 2017 The Authors. Published by Elsevier B.V. This is an open access article under the CC BY license (http://creativecommons.org/licenses/by/4.0/).

1. Introduction

The development of electric vehicles (EV) and hybrid electric (HEV) has been driven in recent years by the desire to be more environmentally friendly. Requirements by governments and consumers for decreases in carbon emissions, improvements in air quality and reduced reliance on fossil fuels has placed an onus on motor manufacturers to improve the fuel efficiency of their vehicles and subsequent reduction of exhaust gas. One method of achieving this in HEVs is through improvement of the efficiency of the EV's traction motor. The functional material in the core of the motors is required to have many and often competing properties outlined in Table 1.

Few materials satisfactorily weigh the different requirements for an electric motor more economically than non-oriented electrical steel (NOES). Mechanical punching, which is low cost and suitable for high volumes, is the most popular cutting method. Therefore, the laminations, used in motor cores are largely produced by punching from NOES sheets.

Electrical steel sheets are measured under conditions of no applied stress, uniform alternating field, in a given direction with a sinusoidal flux waveform as prescribed by international standard IEC60404-2. Many of these assumptions are undermined by the manufacturing process and in particular, the punching of the laminations which introduces plastic and elastic stress/strain resulting in an increase in power loss. The greatest impact is on the narrowest parts such as the teeth where the proportion of the width of the degraded zone at the cut edge to the total width is high, unlike the Epstein, which is stress-relief annealed, or SST test samples which can be as wide as 500 mm.

Punching induces plastic strain which peaks in a region of the order of the sample width from the edge but can extend up to 10 mm from the edge if plastic flow isn't limited [1]. These combine with residual stresses due to the non-uniform distribution of plastic strains, potentially extending over the entire width of the sample. These residual microstresses hinder the motion of domain walls and increase power loss. [2]

The cutting of electrical steel is known to affect the magnetic properties negatively with a pronounced effect in the region close to the cut edge [3–6]. Investigations into the effect of cutting have produced varying estimates for the degradation region depth as the depth varies with material properties, cutting type and methodology [7]. Optical microscopy [8–10] shows clear grain deformation in the first 0.5 mm from the edge of punched samples. Altered domain patterns over 1–5 mm were observed [11] using Kerr microscopy. Micro-indentation showed increases in hardness, which can be used to estimate residual stress, pronounced in the first 0.5–1.0 mm [12,13], but with a gradual increase extending up to 10 mm. Naumoski [14] using the MOKE method, noted changes in domain structure over the first two to three grain rows

---

* Corresponding author.
E-mail addresses: lewisnj1@cardiff.ac.uk (N.J. Lewis), AndersonPI1@cardiff.ac.uk (P.I. Anderson).

Table 1
Driving properties and related core material requirements.

Driving property	Material requirements
High torque for starting	High permeability
Compact and lightweight	Low loss under high frequency
Small rotor/stator air gap	Good workability
High fuel efficiency	Low loss in typical driving ranges
High revolutions	High strength

near the edge. Estimations for the degradation depth can be obtained by dividing samples, to increase the number of cut edges per unit width. Gmyrek [15] divided rings 200 mm OD, 160 mm ID into concentric rings and estimates the depth to be 1.87 mm.

Measurement of the local flux density have been made using search coils with the degradation depth extending up to 10 mm from the edge [16,17]. However, this involves damaging the sample and altering the stress field with the drilling of holes. Non-destructive methods include the needle probe methods or the use of capacitors proposed by Zurek [18]. This method uses conductive paint which cannot be moved easily between measurement locations.

There have been several methods proposed to model the magnetisation profile within a sample taking cutting into account. Vandenbossche et al. [19] used the drop in permeability at the edge and a parabolic function, both experimentally determined from strips cut with a guillotine to increase the number of cut edges. Peksoz [20] used Matlab to find the best fitting function with input parameters obtained with search coils from eight experimental data sets. Siebert [5] who used neutron grating interferometry and the so-called dark field image technique, looked at the flux density across the width of 5 mm wide 2.4% NOES (material grade M330-35A) samples, with the B profile calculated for punched samples having a symmetric parabolic shape and notably different from laser cut samples. Elfgen [21] used the mathematical description of the permeability described in [19] to produce a continuous model to describe the local magnetic properties with model parameters identified from SST measurements on M330-35A samples. These are however laser cut which will have a different distribution profile.

As there is such a variance in both degradation depths and flux density profile due to material, geometry and cut method, being able to validate and compare profiles would be of great importance to designers of electrical machines in the optimisation of their designs as well as refining loss models.

2. Measurement principles

Methods to measure both local B and H include a needle probe and H-coil sensor by Enokizono [22] and Hall sensors have been used to measure the local magnetic field [23,24]. The ease of constructing devices using Hall sensors coupled with their simplicity of use and small sensitive area make them suitable for the measurement of local magnetic field.

Measurements of local flux density have included using search coils, which is based on Faraday's law of induction. The main disadvantage of this method is that it requires the drilling of holes in the sample which can induce significant additional stress and cause local variation in flux density distribution.

The needle probe method which was initially proposed by Werner [25] helps to alleviate some of these concerns by not requiring any drilling of the sample. The needle probe method works by calculating the voltage between two points on the surface of a sample, with the measured voltage assumed to be proportional to the rate of change of the flux density within the sample, between the needle tips. For this to be true several assumptions are made; firstly, that the flux distribution within the sample is symmetrical with

regards to the centre axis parallel to the surface on which the needles are placed; secondly that the spacing between the needles is large compared to the sample thickness so that the sample thickness can be neglected [26,27]. This is rarely an issue in electrical steel where the lamination are usually 0.5 mm or less thick. However, due to the grain structure there will not be exact symmetry between top and bottom halves, the best that can be achieved is a similar distribution in number and size of grains. An increase in average grain size and decreases in needle spacing will result in increased errors.

Studies have shown the needle method can produce local flux density measurements in good agreement with search coils [28] although errors can be introduced if the distance between the needle and the edge doesn't exceed half the lamination thickness [29].

The combining of a needle probe and Hall effect sensor along with an accurate and precise positioning system allows a reproducible non-destructive method that also has flexibility in being able to move the measurement location.

The power loss, measured in W/kg is calculated by integrating the area of the loop and is given by the following equation.

$$P_t = \frac{1}{\rho T} \int_0^T H \frac{dB}{dt} dt \tag{1}$$

where H is the instantaneous tangential component of the field at the surface (A/m) and, in this case measured by a Hall effect sensor. B is the instantaneous value averaged over the cross sectional area of the material. ρ is the density of the material (kg/m^3) and T is the period defined as $T = 1/f$ where f is the frequency.

3. Experimental setup

A system was developed to measure the local magnetic properties of punched electrical steel ring samples. This consisted of a computer controlled, AC magnetising system, developed at Cardiff University, consisting of a desktop PC, National Instruments DAQ PCI 6120, power amplifier and isolation transformer [30].

The local magnetising field, power loss, flux density and permeability of 0.35 mm thick 3.2% Si non-oriented punched electrical steel rings with various inner diameters (ID): (150 mm, 160 mm, 170 mm, 180 mm and 190 mm) and constant outer diameter (OD) 200 mm was measured. Rings were chosen as they more closely replicate motor stators but have a simpler geometry which could be more easily magnetised and by keeping the OD fixed and increasing the ID the proportion of degradation depth, which was assumed to be constant to sample width, was increased.

The samples were placed inside Polyamide PA 2200 cases each additively manufactured to suit the various ring diameters although not in direct contact with the sample as to reduce compressive stress and increase air cooling (Fig. 1).
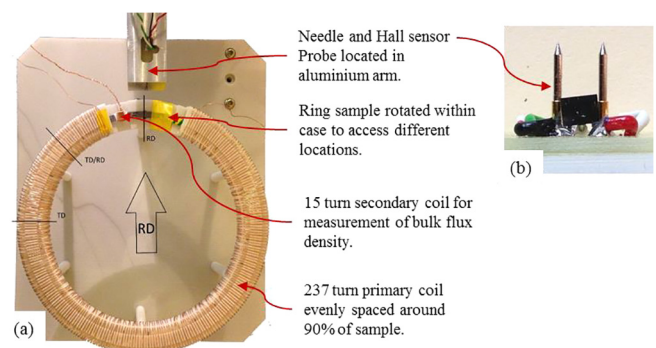
Fig. 1. (a) Plan view of magnetising system for 190 mm ID sample and (b) local measurement probe consisting of Hall effect sensor and needles.

Global magnetic properties were measured using a 0.5 mm thick enamelled copper wire search coil with 15 turns placed on a moveable collar and positioned as close as possible to where the local measurements would be taken. The strength of the magnetising field produced by the coil was calculated using the current, obtained by measuring the voltage across a shunt resistor.

The probe to measure the local properties consisted of two phosphor bronze spring loaded, 2-part, needle tip probes with diameter 1.03 mm and tip separation 2.436 ± 0.024 mm. The needles were spring loaded to ensure a good connection along with the removal of the coating using abrasive paper in the region of interest. The lamination flux density between the needles was calculated from the voltage drop using (2).

$$V = \frac{1}{2} hs \frac{dB}{dt} \tag{2}$$

where h is the lamination thickness and s, the needle separation.

The component of the magnetic field tangential to the sample and perpendicular to the plane of the probe was calculated using (3) with the voltage from a Honeywell SS495A1 series digital Hall-effect sensor located between the needles with the input current provided by the Farnell stabilised DC power supply unit operated at 5 V.

$$H(t) = CV(t) \tag{3}$$

where C is the Hall scaling factor and V is Hall sensor output voltage. The Hall scaling factor which was determined experimentally by placing the Hall effect sensor inside a 1840 turn solenoid and measuring the voltage output at different field strengths as measured by a Lakeshore 480 Fluxmeter also placed inside the 500 mm long solenoid.

Local measurements, repeated three times, were taken at 1 mm intervals and at three locations; perpendicular, parallel and at 45° to the rolling direction across the radial direction of the ring using the probe (Fig. 2). Measurements were taken at the frequencies and globally measured flux density, as measured by the secondary coil shown in Table 2. Measurements have typically been measured at 1.5 T and 50 Hz. However, for high frequency applications such as the tractions motors of HEV which are required to run well above 15000 rpm, results at 1.0 T and 400 Hz are more often used nowadays. Due to the small needle area a relatively weak signal is generated. An increase in the frequency results in an increase in the signal strength and provides more stable measurement conditions. The downside of this however, is a decrease in skin depth and an increase in the non-homogeneity of the flux through the sample.
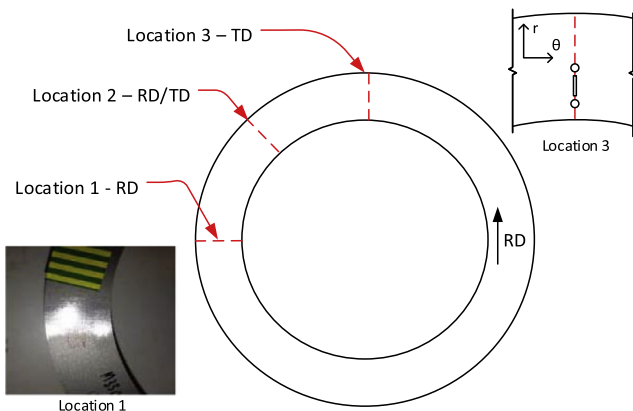
Fig. 2. Schematic of ring sample. The three locations at which measurements were taken were orientated in relation to the rolling direction.

Table 2
Frequencies and global flux densities at which local measurements were taken.

Flux density (T)	Frequency (Hz)
1.0	200/400/800
1.1	200/400/800
1.2	200/400/800
1.3	200/400/800*
1.4	200/400/800*

The computer controlled positioning system was connected to an aluminium arm in which the probe was mounted. The Parker positioning system could move in three dimensions and consisted of a desktop PC running ACR View software.

4. Results and discussion

Similar results were observed for all samples with a typical ring shown in Fig. 3. It shows the results for the Hall probe (a) and the needles (b) taken at a bulk flux density of 1.0 T and at 400 Hz. The magnetising field decreases linearly, moving from the ID edge to the OD edge as would be expected from Ampere's law for a toroid. The field is inversely proportional to the radius, so as the radius increases the field decreases. The anisotropy of the material is clearly seen. Local measurements are taken at a fixed bulk flux density, measured using the secondary coil of 1.0 T with the applied field needed to induce the required flux density approximately 25% higher for measurements in the TD compared to the RD. The process of turning the steel from slabs to sheets, done by cold rolling enhances the growth of [0 0 1] grains in the RD [31].

Proximity to the edge is associated with a decrease in flux density. For the 3.2% Si sample, this change is abrupt and occurs at 2.0 ± 0.5 mm and is consistent with all measurements in the range 1.0 T–1.4 T and 200–800 Hz. The 2.4% Si sample displays a more gradual change. The central dip in flux density observed in some sample can be explained by the large residual stress, at the edge transitioning to smaller compressive and then tensile stress in the centre.

With regards to the legend in Figs. 3 and 4 the bulk measurement is the mean average of the measurements taken at all the locations and directions with H and B calculated from the primary current and secondary coil respectively. Similarly, the local measurement is the mean average of the measurements taken at all the locations and directions and obtained using the Hall effect sensor and needle probe. The difference between the bulk and local measurements could be accounted for by the bulk being measured slightly closer to end of the magnetising coil and additionally influenced by the orientation of the NOES having a greater impact on the local measurements as opposed to the bulk measurements where it is smoothed out over the entire sample.

When the normal of the surface enclosed by the secondary coil is parallel to the RD a higher proportion of the domains have their easy axis also pointing in this direction reducing the field necessary to reach the required flux density. As the secondary coil is moved around the sample to the RD/TD and then TD location, fewer domains have their easy axis parallel to the magnetisation vector. The more complex wall motion requires an increase in the magnetising field to reach the same flux density resulting in the decrease in permeability and increase in power loss seen in the TD as shown in Fig. 4.

The punching of the electrical steel generates plastic stress/strain and increases the number of dislocations localised near the edge. These act as pinning sites impeding the motion of domain walls causing a decrease in the permeability, a measure of how easily a material is magnetised as shown in Fig. 4. This is reflected
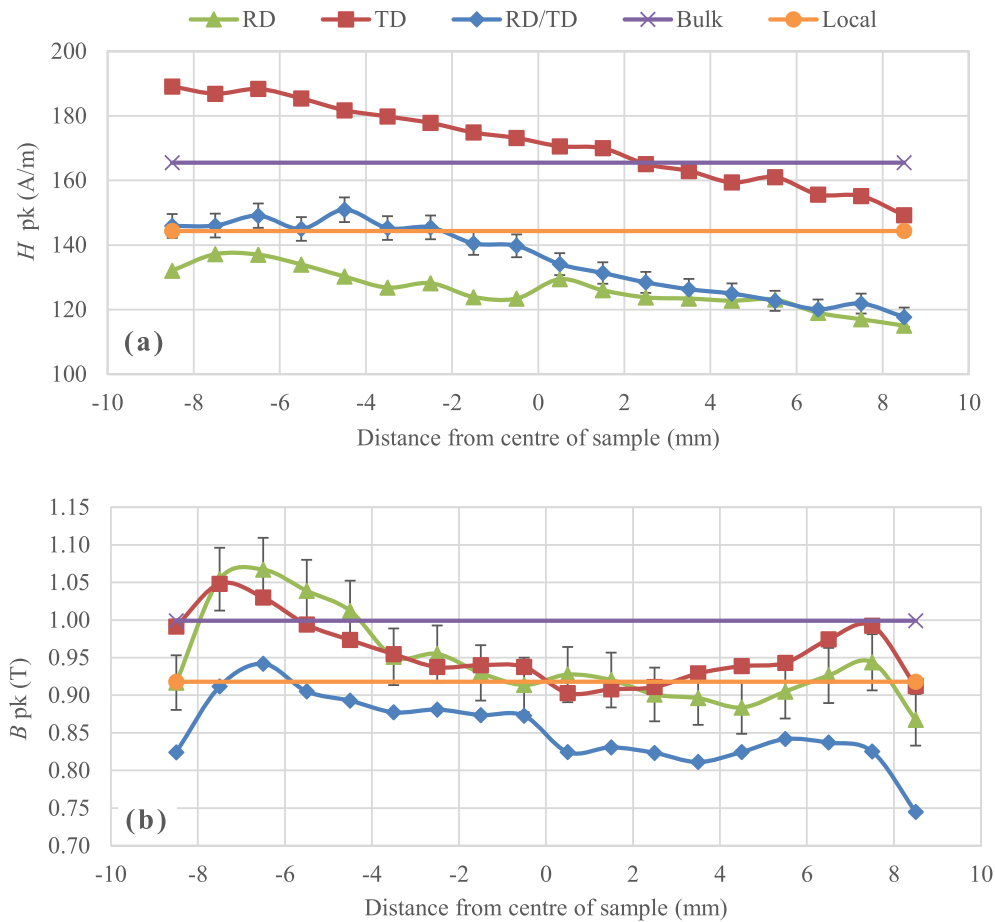
Fig. 3. Local properties, (a) magnetising field and (b) flux density for 20 mm wide (160 mm ID) 3.2% SiFe NOES sample. ID edge at −10 mm and OD edge at 10 mm. Measurements taken at a bulk flux density of 1.0 T 400 Hz. Local is the mean value of local measurements. Bulk is the value obtained from the secondary coil and magnetising current.

in the flux travelling in the more easily magnetised central region as shown with the reduced flux density at the edges. A material with uniform permeability would be expected to have a linear flux density profile which tracts the applied field which is not seen here. The reduction in local flux density and local permeability, calculated using the local B and H (4) can be seen to decrease at the edges and extends approximately 2.5 ± 0.5 mm from the edge which is consistent with reported values including the 1.87 mm by Gmyrek [15] who used the samples with the same geometry.

$$\mu_{r,\text{local}} = \frac{B_{\text{needle probe}}}{\mu_0 H_{\text{Hall sensor}}} \qquad (4)$$

The dip in the centre can be explained by the large residual stress at the edge transitioning to smaller compressive and tensile stresses in the centre. The stress distribution in the plane of a typical cross section can be summarised as follows. There will be large values of residual compressive stress immediately adjacent to the cut edge, which will decrease with distance from the edge sharply at first then more gradually with smaller amounts of compressive stress penetrating into the sample interior before transitioning into tension. This corresponds to a stress profile in the direction of magnetisation consisting of a large tensile component at the edge (reduced permeability) to a small tensile component (increased permeability) which accounts for the peak to finally compression in the centre (reduced permeability) creating the dip in flux density. This central dip is consistent with the upper range of 10–15 mm for the degradation depth reported within the literature and is suggestive of two areas of reduced permeability as opposed to

a continuous decrease.

The magnitude of the change in flux density observed at the edge compared to the centre is related to the location at which it is taken, with the greatest change observed in the RD and the least in the TD. In the RD, increases in magnetisation can be achieved mainly using 180° domain wall motion in the central part of the sample. As the angle to the RD increases and the availability of 180° domain wall motion decreases the flux is forced to use more complex mechanisms located towards the edges.

A decrease in mean permeability with reducing width, shown in Fig. 5 indicates that along with local effects at the edge, longer range stresses acting potentially across the entire width affect the ability to magnetise the sample. This becomes especially important when sample width is smaller than 10 mm. The relative change is also more difficult to detect with decreasing sample width as the needle tip separation becomes a larger proportion of the total width. Measurements are limited to distances greater than half the lamination width from the cut edge as one of the assumptions, zero vertical electric field components, on which the method is based is no longer valid in this region. As the width of the samples gets smaller the proportion of the sample that is inaccessible increases. A possible solution to this would be to decrease the needle tip separation although a decrease of 1 mm would increase the uncertainty in the needle probe area by over 60%.

The effect of punching is dependent on silicon content. The different grades of electrical steel have distinctive profiles. The 3.2% silicon displays an abrupt change in properties at approximately
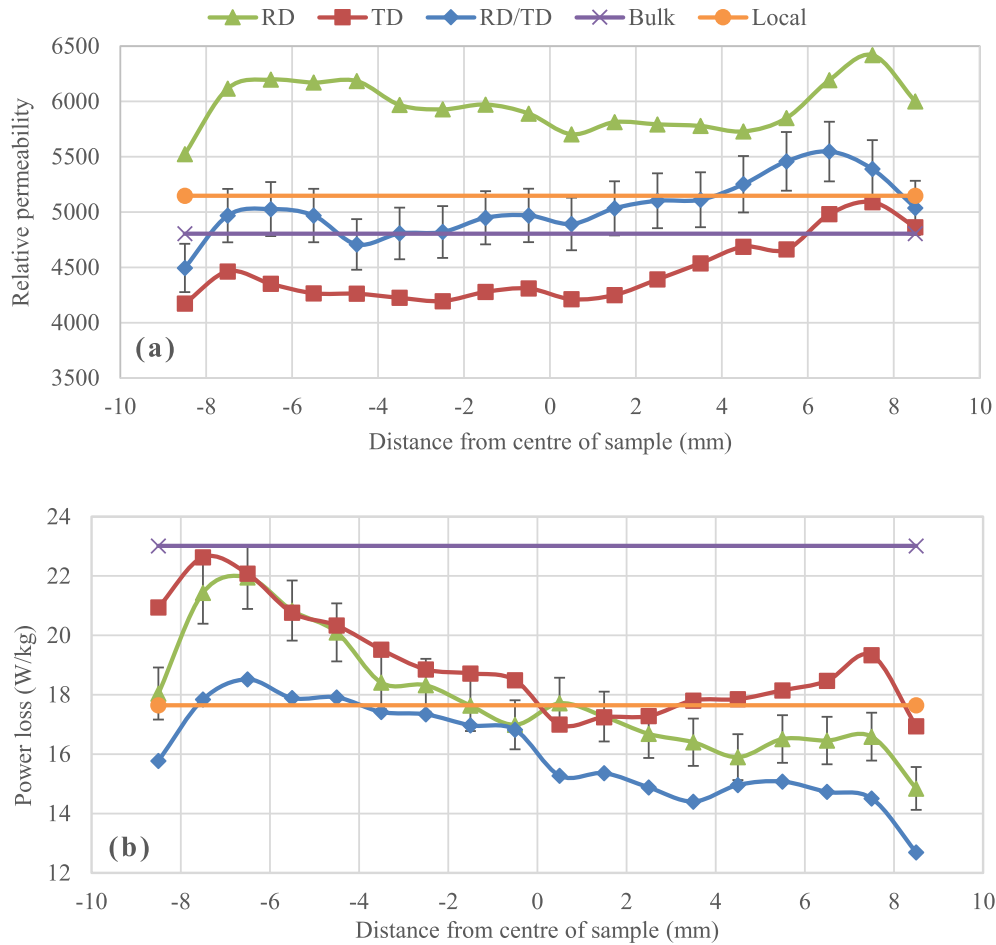
Fig. 4. Local properties, (a) relative permeability and (b) power loss calculated from local H and B measurements for 20 mm wide (160 mm ID) 3.2% SiFe NOES sample. ID edge at −10 mm and OD edge at 10 mm. Measurements taken at a bulk flux density of 1.0 T 400 Hz. Local is the mean value of local measurements. Bulk is the value obtained from the secondary coil and magnetising current.
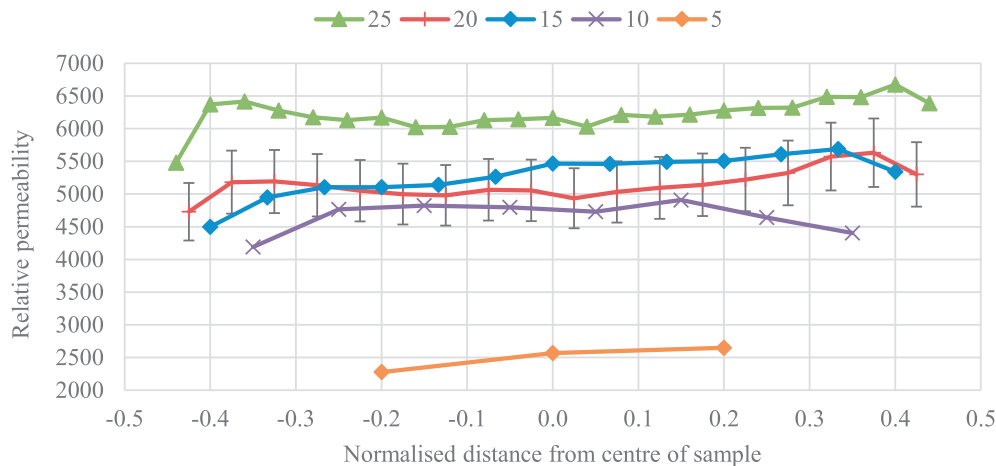
Fig. 5. Permeability profile of the mean average of the three different locations of 3.2% SiFe samples with widths ranging from 55 mm to 5 mm (150–190 mm ID respectively) and normalised over the width of the sample. ID edge at −0.5 and OD edge at 0.5. Measurements taken at a bulk flux density of 1.0 T 400 Hz.

2.5 ± 0.5 mm whereas the 2.4% silicon material displays a more gradual change. A possible explanation could be that the increased silicon is causing more dislocation pile up and reducing plastic flow resulting in a more pronounced effect near the edge (Fig. 6).

Advantages of this system include the relative speed of measurements, low sample preparation time and that it can be applied to a large variety which could include more complex stator designs.

The geometry of the sample and positioning of magnetising coils will dictate the ease at which a uniform magnetising field can be applied and consideration should be given to obtaining stable measurement conditions, which did prove difficult, limiting
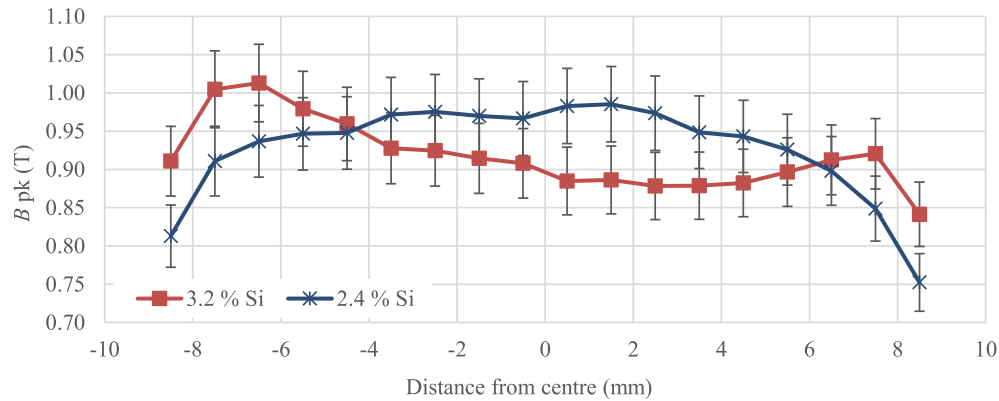
Fig. 6. Average flux density profiles for 2.4% (square) and 3.2% (star) NOES samples for 20 mm wide (160 mm ID). ID edge at −10 mm and OD edge at 10 mm. Measurements taken at a bulk flux density of 1.0 T 400 Hz.

the range of frequencies and flux densities over which measurements could be taken. This system used rings as an approximation to motor stators which has the advantage of creating a uniform magnetic field, for constant radius around 90% of the sample, the field is disrupted by the unavoidable gap necessary for probe access. The magnetising field is not uniform across the width of the sample, decreasing linearly with increasing radius resulting in the other local properties being measured at different applied fields. The magnitude of the gradient increases with both increasing field and angle to the RD increasing uncertainty. Future work could look at using the local magnetising field to determine the measurement points.

The Hall probe records a lower reading when compared to the value calculated from the magnetising coil. A possible explanation for this is that the Hall probe is not located directly on the sample. Future investigation of the decrease in field strength with distance for different geometries and magnetising conditions and the ability to predict the field strength on the surface from nearby measurements would be expected to improve the agreement between the two methods.

5. Conclusion

In this paper, an experimental system was proposed for the non-destructive identification of the variation in local magnetic properties with the simultaneous measurement of the localised magnetising field and flux density of electrical steel rings. This system could accurately and repeatedly select locations on a sample and as a result, this new approach to precision measurement can map the variation in the magnetic properties across an electrical steel sample.

Increasing the silicon content hindered the progression of newly created dislocations into the interior of the sample resulting in a more pronounced degraded zone, 3.2% 0.35 mm thick electrical steel showed a sharp change in permeability extending over approximately 2.5 ± 0.5 mm from the edge. Lowering the silicon content results in a more gradual decrease in permeability over a larger distance.

Unlike other work that only examines the cut edges, looking at the entire sample width showed a permeability dip in the centre of 3.2% silicon samples attributed to the changing nature of the residual stress, which was not observed in 2.4% silicon samples. This allowed for more accurate profiles of the magnetic properties throughout a sample to be obtained with the aim of improving the power loss predictions for electric motors.

References

[1] A. Pulnikov, P. Baudouin, J. Melkebeek, Induced stresses due to the mechanical cutting of non-oriented electrical steels, J. Magn. Magn. Mater. 254–255 (2003) 355–357.
[2] B.D. Cullity, Introduction to Magnetic Materials, Addison-Wesley.
[3] A.J. Moses, N. Derebasi, G. Loisos, A. Schoppa, Aspects of the cut-edge effect stress on the power loss and flux density distribution in electrical steel sheets, J. Magn. Magn. Mater. 215–216 (2000) 690–692.
[4] G. Crevecoeur, L. Dupre, L. Vandenbossche, R. Van de Walle, Local identification of magnetic hysteresis properties near cutting edges of electrical steel sheets, Magn. IEEE Trans. 44 (2008) 1010–1013.
[5] R. Siebert, J. Schneider, E. Beyer, Laser cutting and mechanical cutting of electrical steels and its effect on the magnetic properties, Magn. IEEE Trans. 50 (2014) 1–4.
[6] R. Rygal, A.J. Moses, N. Derebasi, J. Schneider, A. Schoppa, Influence of cutting stress on magnetic field and flux density distribution in non-oriented electrical steels, J. Magn. Magn. Mater. 215–216 (2000) 687–689.
[7] G. Loisos, A.J. Moses, Effect of mechanical and Nd:YAG laser cutting on magnetic flux distribution near the cut edge of non-oriented steels, J. Mater. Process. Technol. 161 (2005) 151–155.
[8] M. Emura, F. Landgraf, W. Ross, J. Barreta, The influence of cutting technique on the magnetic properties of electrical steels, J. Magn. Magn. Mater. 254 (2003) 358–360.
[9] E.G. Araujo, J. Schneider, K. Verbeken, G. Pasquarella, Y. Houbaert, Dimensional effects on magnetic properties of fe–si steels due to laser and mechanical cutting, IEEE Trans. Magn. 46 (2010) 213–216.
[10] Y. Kurosaki, H. Mogi, H. Fujii, T. Kubota, M. Shiozaki, Importance of punching and workability in non-oriented electrical steel sheets, J. Magn. Magn. Mater. 320 (2008) 2474–2480.
[11] K. Senda, M. Ishida, Y. Nakasu, M. Yagi, Influence of shearing process on domain structure and magnetic properties of non-oriented electrical steel, J. Magn. Magn. Mater. 304 (2006) e513–e515.
[12] T. Omura, Y. Zaizen, M. Fukumura, K. Senda, H. Toda, Effect of hardness and thickness of non-oriented electrical steel sheets on iron loss deterioration by shearing process, Magn. IEEE Trans. PP (2015), 1–1.
[13] H. Cao, L. Hao, J. Yi, X. Zhang, Z. Luo, S. Chen, et al., The influence of punching process on residual stress and magnetic domain structure of non-oriented silicon steel, J. Magn. Magn. Mater. 406 (2016) 42–47.
[14] H. Naumoski, B. Riedmüller, A. Minkow, U. Herr, Investigation of the influence of different cutting procedures on the global and local magnetic properties of non-oriented electrical steel, J. Magn. Magn. Mater. 392 (2015) 126–133.
[15] Z. Gmyrek, A. Cavagnino, L. Ferraris, Estimation of the magnetic properties of the damaged area resulting from the punching process: experimental research and FEM modeling, IEEE Trans. Indus. Appl. 49 (2013) 2069–2077.
[16] T. Nakata, M. Nakano, K. Kawahara, Effects of stress due to cutting on magnetic characteristics of silicon steel, Magn. Jpn. IEEE Transl. J. 7 (1992) 453–457.
[17] G. Loisos, A.J. Moses, Variation of magnetic flux density with distance from the cut edge of grain oriented electrical steel, 2006.

[18] S. Zurek, T. Meydan, A novel capacitive flux density sensor, Sens. Actuators A 129 (2006) 121–125.

[19] L. Vandenbossche, S. Jacobs, F. Henrotte, K. Hameyer, Impact of cut edges on magnetization curves and iron losses in e-machines for automotive traction, The 25th World Battert, Hybrid and Fuel Cell Electric Vihicle Symposium & Exhibition, 2010.

[20] A. Peksoz, S. Erdem, N. Derebasi, Mathematical model for cutting effect on magnetic flux distribution near the cut edge of non-oriented electrical steels, Comput. Mater. Sci. 43 (2008) 1066–1068.

[21] S. Elfgen, S. Boehmer, S. Steentjes, D. Franck, K. Hameyer, Continuous model of magnetic material degradation due to cutting effects in the numerical simulation of electro laminations, in: IKMT 2015; 10 ETG/GMM-Symposium Innovative small Drives and Micro-Motor Systems, 2015, pp. 1–6.

[22] M. Enokizono, M. Morikawa, K. Kawamura, J. Sievert, Distribution of two-dimensional magnetic properties in three-phase induction motor model core, IEEE Trans. Magn. 32 (1996) 4989–4991.

[23] X.T. Xu, Localised Variation of Magnetic Properties of Grain Oriented Electrical Steels (PhD), Cardiff University, 2014.

[24] O. Stupakov, System for controllable magnetic measurement with direct field determination, J. Magn. Magn. Mater. 324 (2012) 631–636.

[25] E. Werner, Austrian Patent no 191 015, Austria Patent 191015, 1949.

[26] T. Yamaguchi, K. Senda, M. Ishida, K. Sato, A. Honda, T. Yamamoto, Theoretical analysis of localized magneticflux measurement by needle probe, J. Phys. iv (1998).

[27] M. De Wulf, L. Dupré, D. Makaveev, J. Melkebeek, Needle-probe techniques for local magnetic flux measurements, J. Appl. Phys. 93 (2003) 8271–8273.

[28] K. Senda, M. Ishida, K. Sato, M. Komatsubara, T. Yamaguchi, Localized magnetic properties in grain-oriented electrical steel measured by needle probe method, Electr. Eng. Jpn. 126 (1999) 1–11.

[29] H. Pfutzner, G. Krismanic, The needle method for induction tests: sources of error, Magn. IEEE Trans. 40 (2004) 1610–1616.

[30] S. Zurek, P. Marketos, T. Meydan, A.J. Moses, Use of novel adaptive digital feedback for magnetic measurements under controlled magnetizing conditions, Magn. IEEE Trans. 41 (2005) 4242–4249.

[31] M. Takashima, M. Komatsubara, N. Morito, {001}<210>; texture development by two-stage cold rolling method in non-oriented electrical steel, ISIJ Int. 37 (1997) 1263–1268.